JOURNAL OF MATERIALS SCIENCE 11 (1976) 593–603

Chemical vapour-deposited silicon nitride

Part 1 *Preparation and some properties*

KOICHI NIIHARA, TOSHIO HIRAI
The Research Institute for Iron, Steel and Other Metals, Tohoku University, Sendai, 980, Japan

Pyrolytic Si_3N_4 has been deposited on a graphite substrate, using a mixture of $SiCl_4$, NH_3 and H_2. The pyrolysis is performed with deposition temperatures of 1100 to 1500° C, total gas pressures of 5 to 300 Torr, and flow rates of $H_2 = 700$, $NH_3 = 60$ and $SiCl_4$ (liq.) $= 0.8\ cm^3\ min^{-1}$. Massive amorphous and crystalline pyrolytic forms of Si_3N_4 are prepared at a maximum thickness of 4.6 mm. The effects of deposition conditions on some properties of the deposited products and the dependence of formation of amorphous or crystalline deposits on deposition temperature and total pressure were investigated. The surface and cross-sectional structures show growth cones and oriented crystals which are strongly dependent on the deposition conditions. The thin deposits are translucent; the thick deposits vary in colour from white to black. The silicon content is close to the theoretical composition and independent of the deposition conditions, while the oxygen content increases with decreasing deposition temperature and total pressure. No segregation of silicon and nitrogen at cone boundaries was found.

1. Introduction

Recently, there has been steady interest in developing high temperature structural materials (oxides, carbides, nitrides, etc) with superior chemical, physical and thermochemical properties for use in nuclear reactors, nuclear fusion reactors and high-temperature gas turbine engines. In particular, silicon nitride (Si_3N_4) has been investigated as a material for stator blades of high-temperature gas turbine engines for its high strength at elevated temperatures, extreme hardness, good thermal shock and creep resistance, and chemical inertness [1]. These favourable properties can be considered well established for reaction-sintered and hot-pressed Si_3N_4 bodies.

The chemical vapour-deposition method (CVD) is one of the most useful techniques for preparing products with high density and purity at relatively low temperatures. Most studies on chemical vapour-deposited Si_3N_4 (pyrolytic Si_3N_4, Py–Si_3N_4) have been concentrated on amorphous thin films ($\sim 10^3$ Å) for use as a diffusion mask or an insulator in the fabrication of semiconductor devices [2–9]. When massive Si_3N_4 is prepared by the CVD method, the massive Py–Si_3N_4 will be more useful as a high-temperature structural material than sintered Si_3N_4. From an economic point of view, the application of higher deposition rates to the preparation of Py–Si_3N_4 with excellent properties is preferable. Airey *et al.* [10] prepared amorphous Si_3N_4 coatings (maximum thickness = 0.8 mm) at a maximum deposition rate of 0.4 mm h^{-1} using a $SiH_4 + NH_3/N_2$ (or H_2) system (N_2, H_2: diluent or carrier gas) and also prepared crystalline coatings at a maximum deposition rate of $0.035\ mm\ h^{-1}$ using a $SiCl_4 + NH_3/N_2$ (or Ar) system. The deposition rates employed by other investigators [2–9, 11–17] are only a few microns per hour. Little work dealing with the preparation of Py–Si_3N_4 at deposition rates of over $0.5\ mm\ h^{-1}$ has been reported in the literature.

This paper describes the preparation method of massive Py–Si_3N_4, the effect of deposition conditions on the surface structures of amorphous and crystalline deposits, and some of their properties. The density and the formation mechanisms will be reported in Part 2.

2. Experimental procedure

2.1. Preparation of Py–Si_3N_4

The experimental set-up and the reaction chamber are illustrated in Figs. 1 and 2, respectively. The reaction chamber consists of a water-cooled metal vacuum tube, a water-cooled copper electrode and a graphite heater on which Py–Si_3N_4 is formed. The graphite resistance heater was made of a graphite electrode rod and was shaped to attain uniform temperature, as shown in Fig. 3. In Fig. 3, values of x and y were varied according to the intended deposition temperature (T_{dep}).

After evacuating and flushing with H_2 the reaction chamber (Fig. 2) and the gas lines (Fig. 1), the graphite substrate (Fig. 3) was directly heated

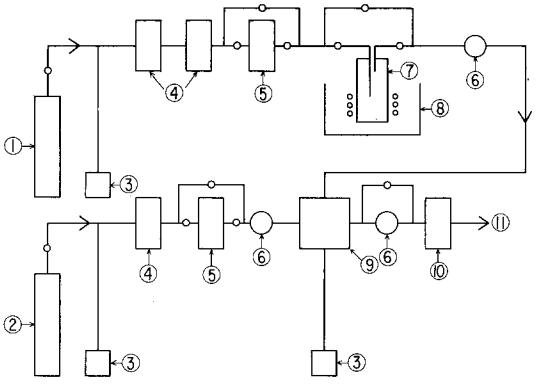

Figure 1 Schematic diagram of Py–Si_3N_4 deposition apparatus. (1) H_2 gas; (2) NH_3 gas; (3) manometer; (4) gas purifier; (5) flowmeter; (6) pressure regulator; (7) $SiCl_4$ reservoir; (8) constant temperature bath; (9) furnace; (10) cold trap; (11) rotary pump.

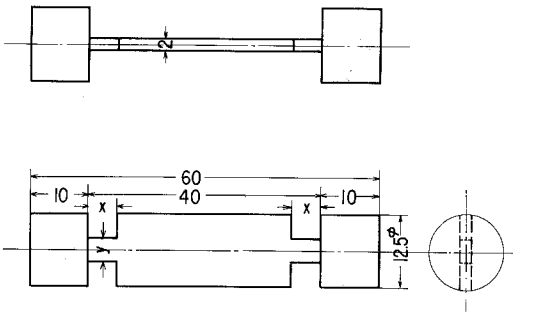

Figure 3 Graphite heater for deposition of Py–Si_3N_4 (x = 5 to 7.1 mm, y = 5.5 to 6.4 mm).

in a stream of H_2 by flow of electric current for 10 min at the desired T_{dep} under reduced pressure, to eliminate volatile impurities in the graphite substrate. The range of T_{dep} was 1100 to 1700° C. A two-colour pyrometer was used for deposition temperature measurements. At the end of a run, the temperature was lowered at a sufficiently slow rate to prevent crack formation in the deposits.

It is well known that in the presence of excess NH_3 in the $SiCl_4 + NH_3$ system, diimide is formed even below room temperature by the reaction of $SiCl_4$ with NH_3. Diimide polymerizes readily and various kinds of complex intermediates are formed depending on the imposed temperatures [1–3]. Thus, NH_3 and $SiCl_4 + H_2$ were separately introduced into the reaction chamber to minimize the formation of diimide as shown in Fig. 2 points 3 and 4. It seems likely that the preparation of Py–Si_3N_4 is affected by the total pressure of gases (P_{tot}) in the reaction chamber, because the form-

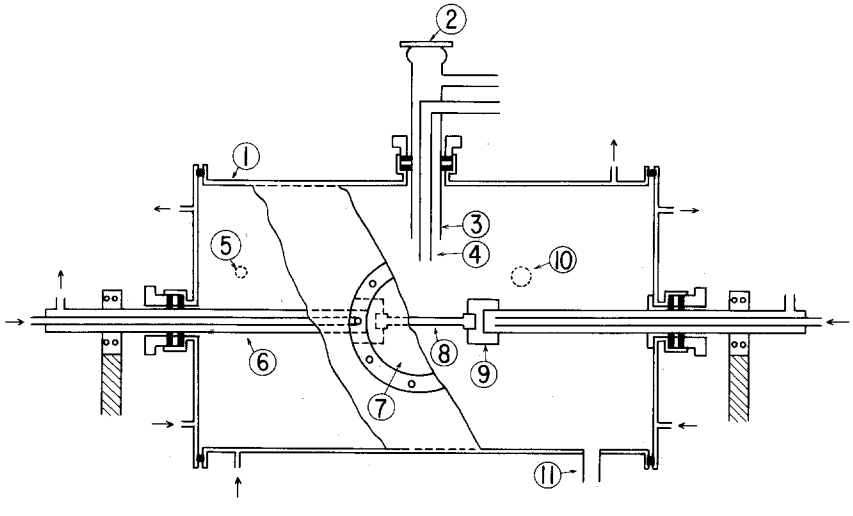

Figure 2 Furnace for Py–Si_3N_4 deposition. (1) Water-cooled vacuum tube; (2) quartz glass window; (3) quartz glass inlet for $SiCl_4 + H_2$; (4) quartz glass inlet for NH_3; (5) pressure gauge; (6) copper electrode; (7) quartz glass window; (8) graphite heater (substrate); (9) graphite socket; (10, 11) gas outlets.

ation and polymerization of diimide proceed through intercollisions of the raw gases or intermediates. Most of the previous work has been performed using atmospheric pressure [2–15] or low P_{tot} (2×10^{-3} to 10 Torr) [16–20]. Unfortunately, there seem to be almost no systematic investigations of the relation between P_{tot} and the formation behaviour and properties of Py–Si_3N_4. In the present experiment, P_{tot} was varied from 5 to 300 Torr.

In analogy with the effect of P_{tot}, the distance between the outlets of the two feed lines (points 3 and 4 in Fig. 2) and the substrate (point 8 in Fig. 2) is an important factor in successfully producing the deposits. The optimum positions of outlets of NH_3 and $SiCl_4 + H_2$ are 2 and 3 cm away from the substrate, respectively. In the 4 to 20 cm range the rate of ammonolysis of $SiCl_4$ was slow, while for a distance of 1.5 cm the thickness of Py–Si_3N_4 was not uniform. In the 2 to 4 cm range, the deposition rate was relatively high and the thickness varied by only about 5% across a 2 cm^2 area of the deposits.

Slow flow rates of NH_3 were employed in order to prevent the formation of diimide and the destruction of the graphite substrate by absorption of NH_3 during the deposition. Calibrated flowmeters were used to meter the amounts of H_2 and NH_3. The vapour of $SiCl_4$ was carried into the chamber by bubbling H_2 through the liquid $SiCl_4$. A $SiCl_4$ reservoir was maintained at 20° C. Flow rates of H_2, NH_3 and $SiCl_4$ were fixed at 700, 60 and 0.8 (in liquid) $cm^3 min^{-1}$, respectively. The deposition was done for 0.5 to 10 h. The purities of $SiCl_4$, NH_3 and H_2 were 99.9, 99.9 and 99.9999% respectively.

2.2. Observation of Py–Si_3N_4

2.2.1. Microscopic observation

The Py–Si_3N_4 formed was mounted in resin, cut perpendicular to the deposition surface and polished by an ordinary metallographic technique. The cross-section of the deposits was examined under polarized light or differential interference conditions. As-deposited surfaces were also examined.

2.2.2. Scanning electron microscopic observation

The as-deposited surface was coated with gold (50 to 100 Å in thickness) and examined in a SEM at magnifications x 100 to x 20000.

2.2.3. X-ray diffraction analysis

X-ray measurements were made with a diffractometric unit using Ni-filtered Cu$K\alpha$ radiation on powdered samples (200 to 325 mesh).

2.2.4. Electron probe microanalysis

The polished deposition and cross-sectional surfaces of the deposits, coated with gold (50 to 100 Å thick), were observed by means of electron probe microanalysis. Contents of silicon, nitrogen and oxygen in the deposits were calculated using the following equation:

$$C_{Si,N,O} = (K_{Si,N,O} - K_B)/[K_{(Si,N,O)} - K_{(B)}]$$

where C = content of each element in the deposits; K = counts of each element in the deposits, K_B = counts of background in the deposits; and $K_{(\,)}$ = standard counts in the standard samples. Standard samples used for silicon, nitrogen and oxygen analyses were high-purity silicon, BN and Al_2O_3 single crystal, respectively. The measurements were made under the following conditions: Si$K\alpha$ (7.126 Å), N$K\alpha$ (31.603 Å), O$K\alpha$ (23.707 Å); accelerating voltage = 10 kV; sample current = 0.1 μA.

3. Results

As shown in Fig. 4, two types of Py–Si_3N_4 (amorphous and crystalline deposits) were obtained in the present experiments. These depended markedly on T_{dep} and P_{tot}. At T_{dep} below 1200° C, amorphous deposits were formed on the graphite substrate over the whole range of P_{tot} (region A) studied. The maximum thickness of an

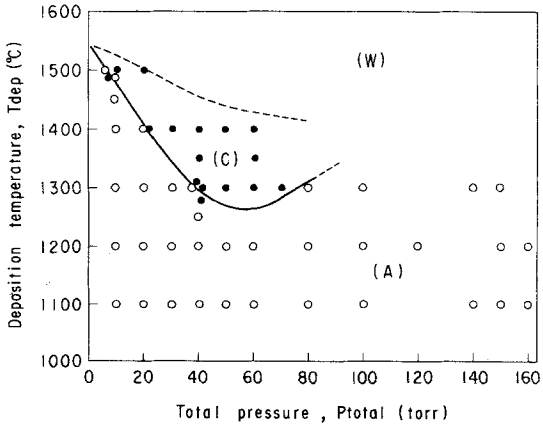

Figure 4 Effect of the deposition temperature (T_{dep}) and the total pressure (P_{tot}) on the structure of Py–Si_3N_4. (A) Amorphous Py–Si_3N_4; (C) crystalline Py–Si_3N_4; (W) no deposits (whisker or needle-like Si_3N_4).

amorphous deposit was 4.2 mm. At 1300° C, the structure depended on P_{tot}; it was amorphous at P_{tot} below 40 Torr and above 75 Torr, while crystalline between 40 and 75 Torr. At 1400 and 1500° C, crystalline deposits were obtained above 20 and 5 to 10 Torr, respectively (region C). The maximum thickness of a crystalline deposit was 4.6 mm.

X-ray diffraction patterns of amorphous and crystalline deposits are included in Fig. 5a and b, respectively. Detailed analysis of the X-ray results indicates that all the crystalline deposits are a hexagonal type α–Si_3N_4 belonging to the P31c space group [21, 22].

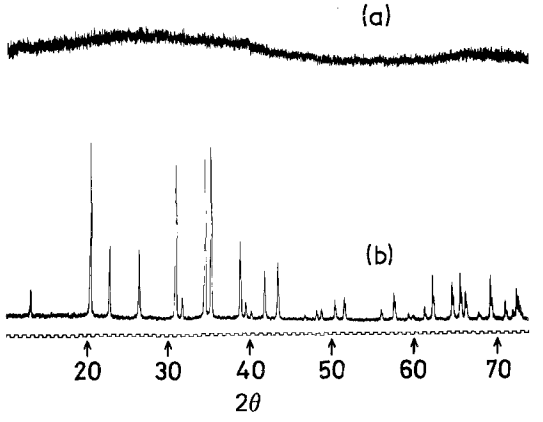

Figure 5 Typical X-ray diffraction patterns. (a) Amorphous Py–Si_3N_4 (T_{dep} = 1300° C, P_{tot} = 30 Torr); (b) crystalline Py–Si_3N_4 (T_{dep} = 1400° C, P_{tot} = 40 Torr); (Cu$K\alpha$ radiation filtered with Ni).

To confirm homogeneity of the deposits, electron probe microanalysis was carried out on the deposition and cross-sectional surfaces. Special attention was taken to observe whether or not segregation of silicon in cone boundaries took place. Fig. 6 shows the results obtained for amorphous deposits; the positions of the cone boundaries are marked by arrows. No changes in silicon and nitrogen contents were observed at the cone boundaries in either the cross-sectional or the deposition surface. The results for crystalline deposits were similar to those for amorphous deposits. The results indicates that the deposits were homogeneous and that silicon does not segregate in the cone boundaries.

The silicon and oxygen contents of Py–Si_3N_4 determined by electron probe microanalysis are summarized in Table I, which also includes the structures and colours of the deposits. The silicon contents of amorphous and crystalline deposits were close to the theoretical composition (60.08 wt %) as indicated in Table I. The composition of the deposits prepared in this experiment is seen to correspond to stoichiometric Si_3N_4. However, the oxygen content increased with decreasing T_{dep} and P_{tot}, and was higher in the amorphous deposits than in the crystalline deposits.

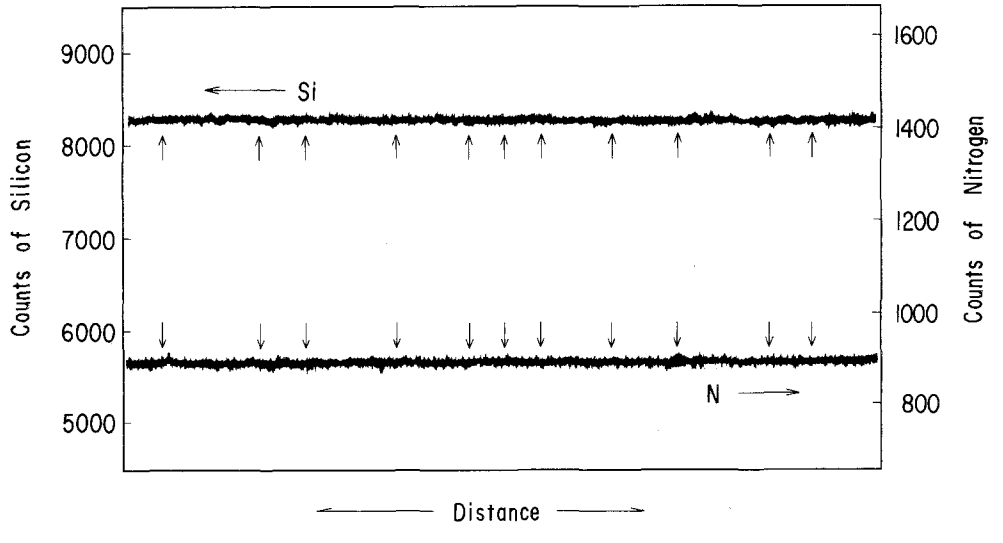

Figure 6 The results of electron probe microanalysis for silicon and nitrogen contents of the amorphous deposit surface prepared at T_{dep} = 1200° C and P_{tot} = 40 Torr. ↓, the position of the cone boundaries.

TABLE I Composition and colour of Py–Si_3N_4 prepared under various conditions.

Deposition conditions		Composition (wt %)		Structure*	Colour
T_{dep} (°C)	P_{tot} (Torr)	Silicon	Oxygen		
1200	40	59.1	2.2	A	white
1300	20	58.8	2.1	A	white
1300	40	60.3	0.7	A + C	dark brown
1300	50	59.4	0.6	C	brown
1300	60	59.2	0.4	C	purple
1400	10	58.8	1.6	A	white
1400	30	59.7	0.6	C	brown
1400	50	59.6	0.3	C	black
Theoretical composition		60.08	0		

*A: amorphous, C: crystalline (α-Si_3N_4).

3.1. Amorphous Py–Si_3N_4

As shown in Fig. 5, X-ray diffraction patterns of the deposits prepared in region A in Fig. 4 indicate that the deposits had amorphous structures. Examples of amorphous Py–Si_3N_4 (with the graphite substrates) are shown in Fig. 7. Amorphous deposits prepared under the various conditions were translucent in thin deposits (Figs. 7A and 8) and showed a white colour and metallic brightness in thick deposites (Fig. 7B). The brightness increased with T_{dep}. The degree of translucence decreased with increase in thickness.

Surface structures of amorphous deposits may be divided into three types, as shown in Figs. 9 to 11. The first typical surface structure was formed at low T_{dep} below 1200° C and low P_{tot} below 20 Torr. An example is shown in Fig. 9. Only the primary pebble structure can be observed in the deposits. The pebble structure corresponds to the top of growth cones. Fig. 10 shows the second typical surface structure which was obtained over the range of higher T_{dep} and P_{tot} in region A. In this case, large primary cones are composed of

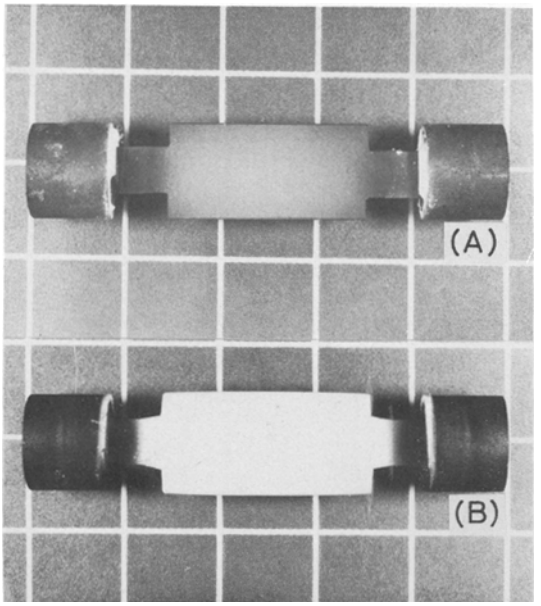

Figure 7 Amorphous Py–Si_3N_4 (1 division = 13 mm). (A) T_{dep} = 1100° C, P_{tot} = 10 Torr; 2 h; (B) T_{dep} = 1300° C, P_{tot} = 30 Torr, 3 h.

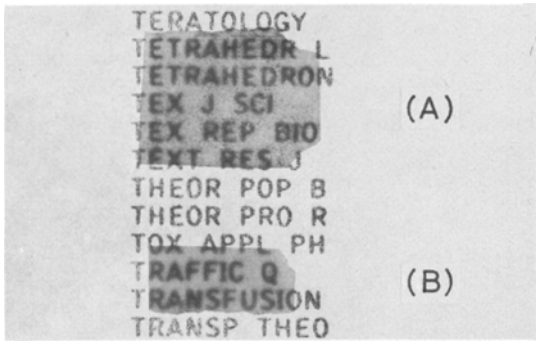

Figure 8 Translucent amorphous Py–Si_3N_4. (A) T_{dep} = 1200° C, P_{tot} = 10 Torr, 2 h, thickness = 0.085 mm, colour = white; (B) T_{dep} = 1300° C, P_{tot} = 80 Torr, 3 h, thickness = 0.090 mm, colour = white.

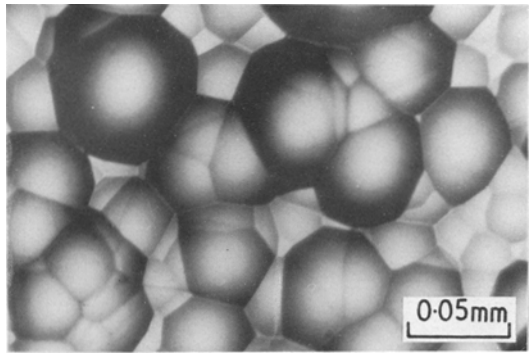

Figure 9 Surface structure of amorphous Py–Si_3N_4 prepared at T_{dep} = 1200° C and P_{tot} = 10 Torr.

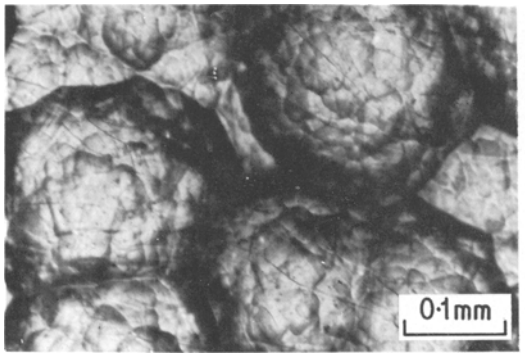

Figure 10 Surface structure of amorphous Py–Si_3N_4 prepared at T_{dep} = 1300° C and P_{tot} = 30 Torr.

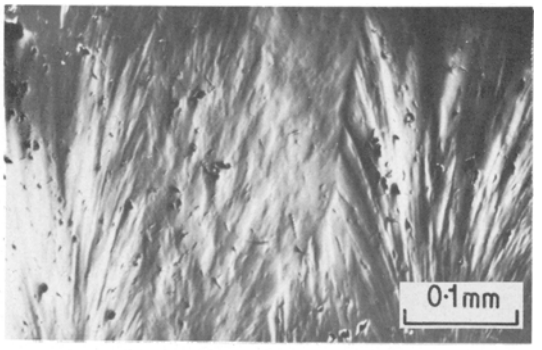

Figure 12 Cross-sectional structure of the amorphous deposit prepared at T_{dep} = 1300° C and P_{tot} = 30 Torr.

secondary cones. Figs. 11a and b indicate the third typical surface which was found in the amorphous deposits prepared at the boundary zone between regions A and C. Large primary cones include numerous small secondary pebble-like cones. The surface of secondary cones (Fig. 11b) is smooth and similar to that in Fig. 9.

An example of the cross-sectional structure is shown in Fig. 12. This cross-sectional structure was observed in the deposits with the surface structure of Fig. 10. The primary and secondary cone boundaries are confirmed in this figure. In the deposits with the surface structure of Fig. 9, the cone boundaries were not detected clearly.

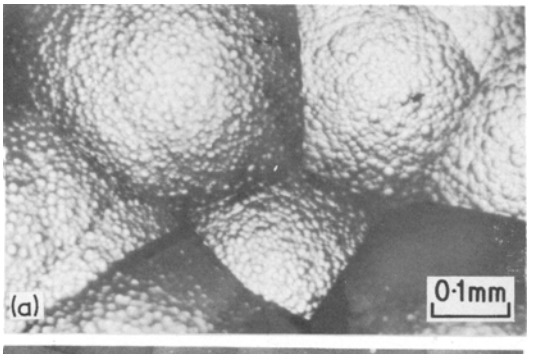

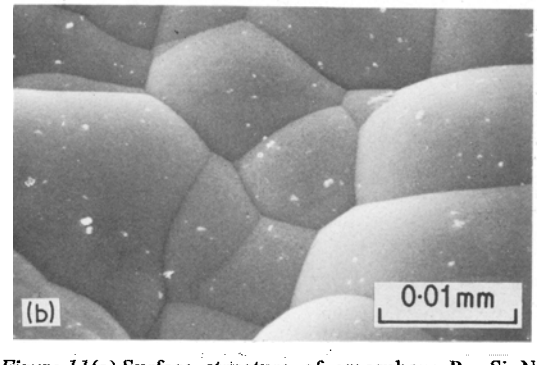

Figure 11 (a) Surface structure of amorphous Py–Si_3N_4 prepared at T_{dep} = 1400° C and P_{tot} = 20 Torr. (b) Scanning electron micrograph of (a) at higher magnification.

3.2. Crystalline Py –Si_3N_4

Fig. 5b shows that the crystal structure of crystalline Py–Si_3N_4 prepared in region C is the α-type hexagonal structure. Amorphous Py–Si_3N_4 was white as described already, while the surface of crystalline deposits was white, brown, dark purple and black depending on the deposition process conditions as listed in Table I. Thin crystalline deposits were also translucent as shown in Fig. 13. An example of a crystalline deposit with the graphite substrate is shown in Fig. 14. In some cases

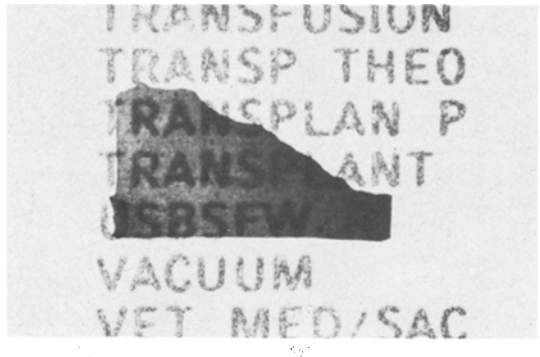

Figure 13 Translucent crystalline Py–Si_3N_4. T_{dep} = 1300° C, P_{tot} = 60 Torr, 2 h, thickness = 0.22 mm, colour = brown.

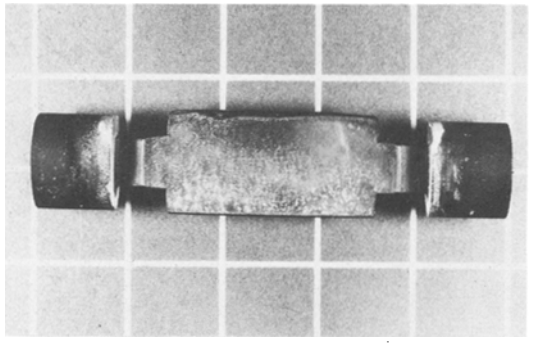

Figure 14 Crystalline Py–Si_3N_4 (1 division = 13 mm). T_{dep} = 1300° C, P_{tot} = 60 Torr, 2 h.

the crystalline deposits showed the marked brightness resulting from a preferred orientation of grains. The relation between the preferred orientation and deposition conditions will be reported elsewhere.

Surface structures of crystalline deposits were remarkably different from those of amorphous deposits, and depended strongly on deposition conditions, as shown in Figs. 15 to 17.

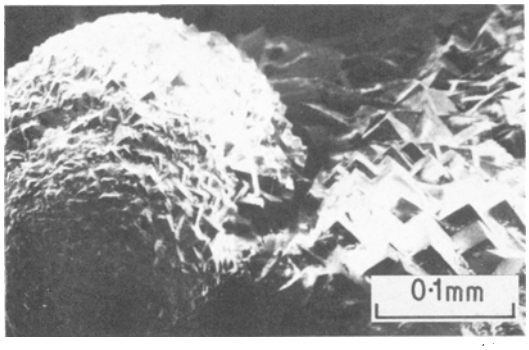

Figure 15 Scanning electron micrograph of the surface of Py–Si_3N_4 prepared at $T_{dep} = 1300°$ C and $P_{tot} = 50$ Torr.

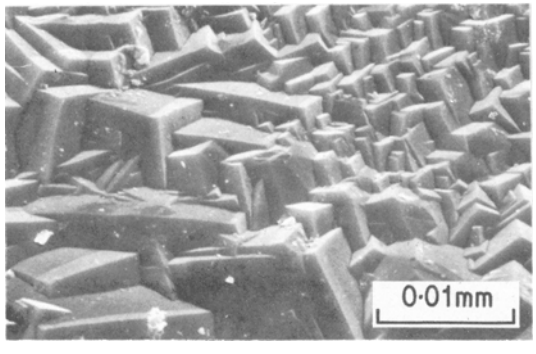

Figure 16 Scanning electron micrograph of the surface of Py–Si_3N_4 prepared at $T_{dep} = 1300°$ C and $P_{tot} =$ 60 Torr.

At $T_{dep} = 1300°$ C, surface structures varied with P_{tot}. At $P_{tot} = 50$ Torr (Fig. 15), growth cones were observed (two cones in Fig. 15) and each cone was composed of a number of small crystals which had well-defined corners (near 90°). At $P_{tot} = 60$ Torr (Fig. 16), no growth cones were found and the whole surface was made up of well-defined crystals. The surface of each crystal was smooth. It is obvious from Fig. 16 that the faceted growth occurs and that each grain has nearly the same orientation. At $P_{tot} = 70$ Torr, the presence of primary and secondary growth cones was observed as shown in Fig. 17a. However, the secondary growth cone was composed of small crystals of varying type (Fig. 17b). The results mentioned above imply that growth cones appear near the A–C boundary (see Fig. 4).

At $T_{dep} = 1400°$ C, the surface structures are shown in Figs. 18 to 21. At $P_{tot} = 20$ Torr (near the A–C boundary), growth cones were composed of small crystals (Fig. 18a). Not all crystal surfaces were smooth and not all sharp (Fig. 18b), in contrast to those in Fig. 16. Fig. 19 shows that the deposits prepared at $P_{tot} = 30$ Torr have well-defined crystals with no growth cones, as in the case of Fig. 16. At $P_{tot} = 50$ Torr, Fig. 20 reveals a different type of crystal growth in which another crystal face exists at the edge of almost each small crystal.

At $T_{dep} = 1500°$ C, Fig. 21a shows growth cones composed of small crystals, as obtained at $P_{tot} = 10$ Torr. The surface of the crystal is not smooth and seems to be corrugated.

Fig. 22 indicates the typical cross-sectional structure of crystalline deposits. Similar structure was observed in all the crystalline deposits.

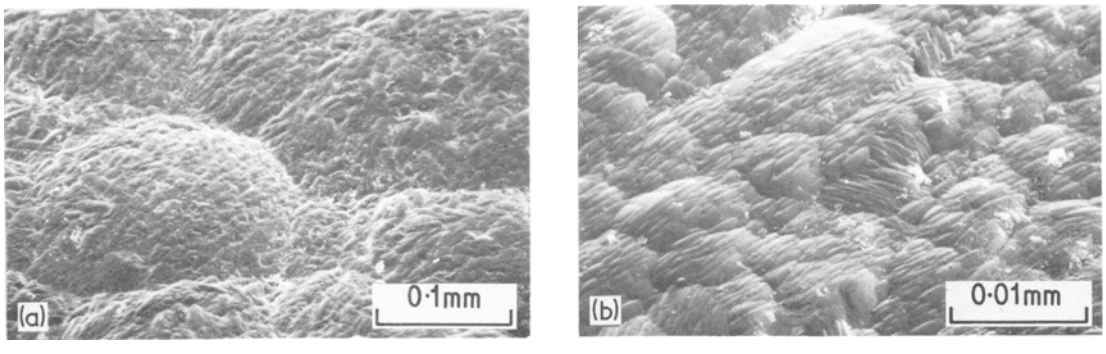

Figure 17(a) Scanning electron micrograph of the surface of Py–Si_3N_4 prepared at $T_{dep} = 1300°$ C and $P_{tot} = 70$ Torr. (b) Higher magnification of (a).

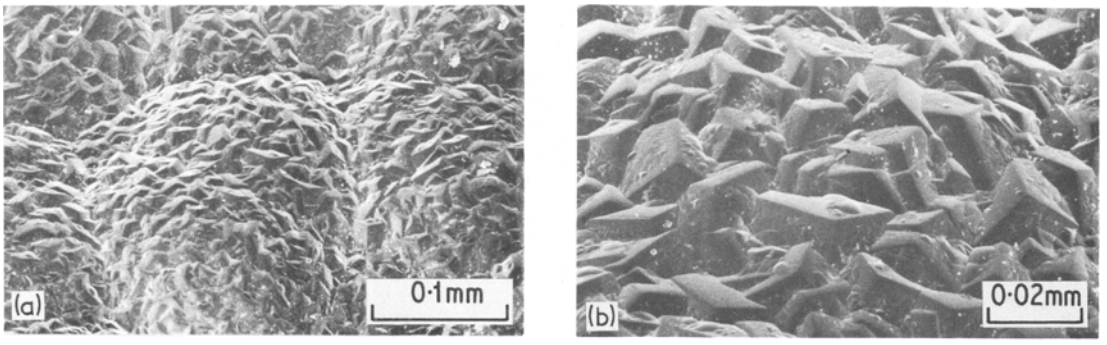

Figure 18(a) Scanning electron micrograph of the surface of Py–Si_3N_4 prepared at $T_{dep} = 1400°$ C and $P_{tot} = 20$ Torr. (b) Higher magnification of (a).

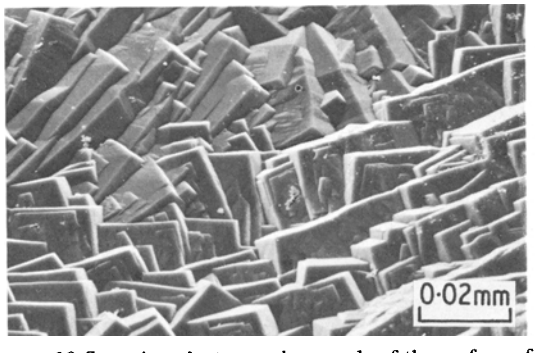

Figure 19 Scanning electron micrograph of the surface of Py–Si_3N_4 prepared at $T_{dep} = 1400°$ C and $P_{tot} = 30$ Torr.

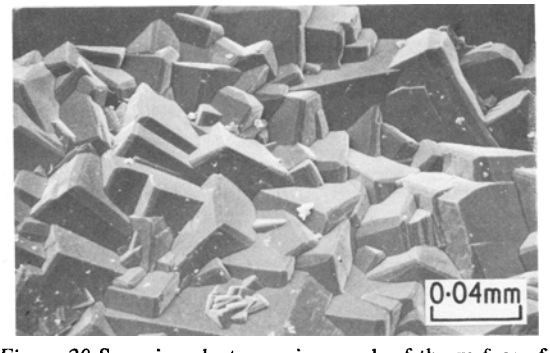

Figure 20 Scanning electron micrograph of the surface of Py–Si_3N_4 prepared at $T_{dep} = 1400°$ C and $P_{tot} = 50$ Torr.

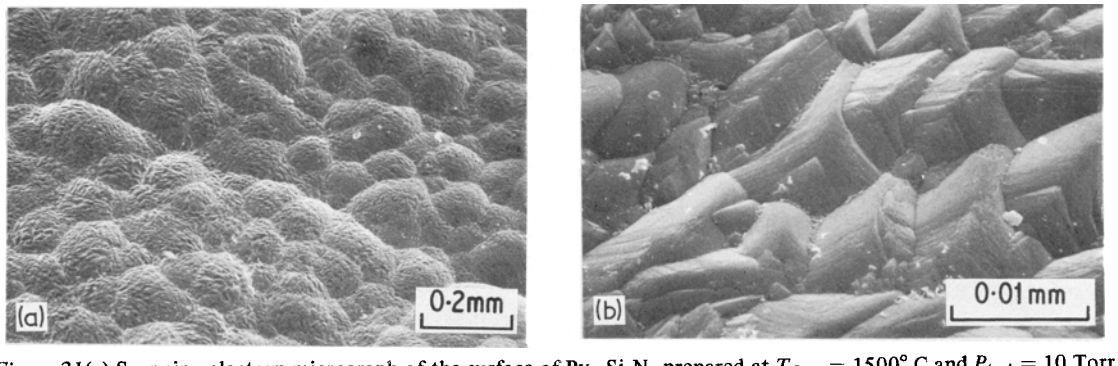

Figure 21(a) Scanning electron micrograph of the surface of Py–Si_3N_4 prepared at $T_{dep} = 1500°$ C and $P_{tot} = 10$ Torr. (b) Higher magnification of (a).

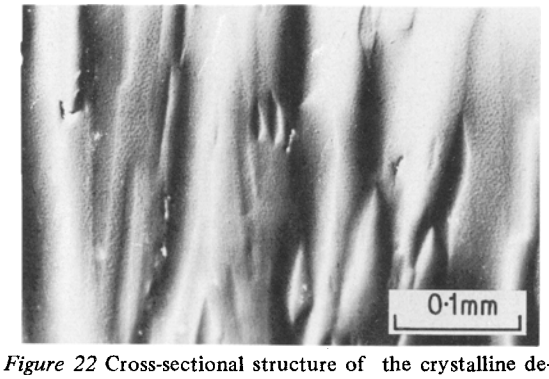

Figure 22 Cross-sectional structure of the crystalline deposit prepared at $T_{dep} = 1400°$ C and $P_{tot} = 50$ Torr.

4. Discussion

4.1. Preparation of Py–Si_3N_4

Py–Si_3N_4 can be prepared by reacting Si or SiH_4 with N_2, NH_3 or N_2H_4 and also silicon halides with $N_2 + H_2$ mixtures, NH_3 or N_2H_4. Most of the previous work on the preparation of Py–Si_3N_4 has been done using SiH_4 [3, 11–13, 22] and $SiCl_4$ [2, 3, 12–14] which have sufficient vapour pressures at room temperature. $SiCl_4$ is inexpensive, safe and easy to handle compared with SiH_4. Moreover, $SiCl_2$ produced from $SiCl_4$ in the gas phase and $SiCl_4$ are relatively stable and can only be completely reduced by excess H_2 [23]. Reactions

TABLE II Experimental data on Py–Si_3N_4 deposition

Reference	Reactants/carrier	T_{dep} (°C)	P_{tot} (Torr)	Thickness (mm)	Structure†
Chu *et al.* [3]	$SiCl_4 + NH_3/H_2$	1000~1200	760	F*	A
Bean *et al.* [12]	$SiH_4 + NH_3/H_2$	600~1400	760	F*	A + C
Galasso *et al.* [17]	$SiF_4 + NH_3$	1100~1550	1 ~ 10	–	C
Airey *et al.* [10]	$SiH_4 + NH_3/N_2$ (H_2)	800~1200	760	0.8	A
	$SiCl_4 + NH_3/N_2$ (Ar)	1100~1380	760	–	A + C
This work	$SiCl_4 + NH_3/H_2$	1100~1500	5 ~ 300	4.2	A
	$SiCl_4 + NH_3/H_2$	1300~1500	5 ~ 70	4.6	C

* F: thin film (in the order of 10^{-3} mm), † A: amorphous, C: crystalline (α-Si_3N_4).

of silicon halides with NH_3 are more favourable than those with N_2, because the free energy of formation of NH_3 is higher than that of N_2. The choice of NH_3 is also advantageous kinetically; N_2 is chemically inert owing to the large bond energy in the molecule [3], while NH_3 is chemically active. Consequently, the $SiCl_4 + NH_3/H_2$ system was chosen in the present experiments.

The experimental data which have realized the relatively high deposition rates are listed in Table II. Up to the present, the thickest Py–Si_3N_4 coating of 0.8 mm was achieved by Airey *et al.* [10]. In the present experiments, however, Py–Si_3N_4 up to 4.6 mm thick is prepared at a deposition rate of 0.73 mm h^{-1}.

4.2. Formation of whisker or needle-like Si_3N_4

At high T_{dep} and P_{tot} (region W in Fig. 4) no deposit was formed on the graphite substrate, while whisker or needle-like Si_3N_4 were grown on the upper part of the substrate. This material was found to be a single crystal. The maximum size of a crystal was 1.5 mm diameter and 15 mm long. The growth direction seems to be related to the decomposition zone of gas phases. Details of this material will be described elsewhere.

4.3. Heterogeneous Py–Si_3N_4

Deposits of mixed amorphous and crystalline structures were obtained at $T_{dep} = 1400°$ C and $P_{tot} = 20$ Torr and $T_{dep} = 1300°$ C and $P_{tot} = 40$ Torr (A–C boundary). The formation of heterogeneous deposits is probably due to a heterogeneous distribution of some gaseous species in the gas phase. In some runs, the crystalline deposits were formed on amorphous layers.

4.4. Surface structure of Py–Si_3N_4

The pebble structure of an amorphous deposit, shown in Fig. 9, bears a close resemblance to that observed in siliconated pyrolytic graphite [24]. As shown in Fig. 9, the boundary lines among the cones intersect with each other at an angle of about 120°. This fact may suggest that the deposit is formed through a liquid state, as discussed in the previous work [24].

In most of the crystalline deposits, the surface formed at the edge of the substrate (Fig. 23) is different from that at the flat part of the substrate. The crystals shown in Fig. 23 have curved faces that seem to arise from the difference of gas flow patterns.

An inspection of Figs. 9 to 11 and 15 to 21 shows that the surface structure of amophous and

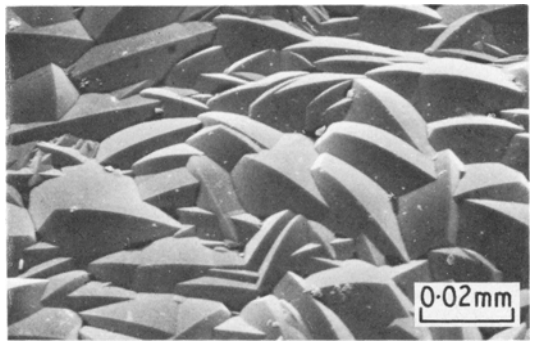

Figure 23 Scanning electron micrograph of the surface of Py–Si_3N_4 prepared at $T_{dep} = 1300°$ C and $P_{tot} = 60$ Torr.

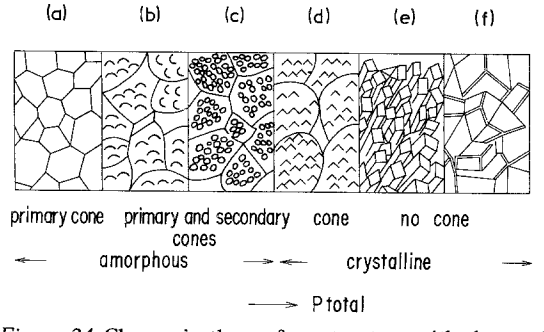

Figure 24 Change in the surface structure with the total pressure (P_{tot}). (a) See Fig. 9; (b) see Fig. 10; (c) see Fig. 11a; (d) see Fig. 15; (e) see Fig. 16; (f) see Fig. 20.

crystalline deposits depends strongly on P_{tot}, which is summarized in Fig. 24.

Airey *et al.* [10] reported that all amorphous coatings prepared by reacting SiH_4 or $SiCl_4$ with NH_3 at atmospheric pressure showed a botryoidal texture which varied according to T_{dep}; at T_{dep} = 900° C ($SiH_4 + NH_3$) the botryoids were an open "cauliflower" type composed of smaller clusters of particles (cf. Fig. 10), while at T_{dep} = 1100 to 1300° C ($SiCl_4 + NH_3$) the botryoids appeared to be dense. They also obtained crystalline deposits with well-rounded botryoids and clusters at ~0.02 mm h^{-1} and 1300° C, and with no botryoidal structure at ~0.012 mm h^{-1} at 1330° C. Galasso *et al.* [17] observed a surface structure similar to that in Fig. 16 on Py–Si_3N_4 prepared by reacting SiF_4 with NH_3 at T_{dep} = 1100 to 1500° C and P_{tot} = 1 to 10 Torr.

4.5. Cross-sectional structure of Py–Si_3N_4

Airey *et al.* [10] reported that the polished and etched cross-section was completely featureless. There seem to be no reports on the cross-sectional structure of Py–Si_3N_4. In this work, as shown in Fig. 12, primary and secondary cone boundaries were revealed for amorphous deposits. However, the cone boundaries of amorphous deposits with only primary cones (Fig. 8) were barely detectable. Also for siliconated pyrolytic graphite [24], cone boundaries of deposits with similar surface structure were not observed clearly. For crystalline deposits, the cross-sectional structure (Fig. 22) suggests the preferred orientation of crystals.

4.6. Cracking in Py–Si_3N_4

All of amorphous deposits were adherent to the graphite substrate. However, it was observed by means of SEM that all amorphous deposits included cracks and that cracks were formed during the deposition. The amount of cracks decreased with increasing T_{dep}.

On the other hand, all the crystalline deposits obtained at T_{dep} = 1300° C were uncracked and adherent to the graphite substrate, and those at T_{dep} = 1400° C and P_{tot} below 70 Torr were uncracked but non-adherent. The crystalline deposits at T_{dep} = 1400° C and P_{tot} above 70 Torr or in region W in Fig. 4 were flaky and exfoliated during the deposition. X-ray diffraction examination identified the thin film of β-SiC with a green colour between the graphite substrate and the deposits at T_{dep} above 1400° C. Therefore, the fact that crystalline deposits were non-adherent or flaky above 1400° C is attributed to the reaction between the graphite substrate and Si_3N_4 deposits.

Many workers on thin amorphous films reported that the cracking occurred in any amorphous deposits whose thickness exceeded 0.001 mm. Kohler [15] reported that the critical thickness of the crack free-film was 1800 Å for the $SiCl_4 + NH_3/H_2$ system and that cracks were initiated at impurity particles at the substrate-nitride interface in most cases. Other workers [4, 8, 13, 15, 25] attributed the cracking to structural changes, composition changes, thermal expansion mismatch within the deposit and between the substrate and the film, and initial substrate conditions.

4.7. Composition of Py–Si_3N_4

Wild *et al.* [26], Colquhoun *et al.* [27] and Feld *et al.* [28] deduced that α-Si_3N_4 had a composition range of $Si_{11.4}N_{15}O_{0.3}$ (0.90 wt % oxygen) and $Si_{11.5}N_{15}O_{0.5}$ (1.48 wt % oxygen) by X-ray, chemical and thermodynamic analyses.

However, Priest *et al.* [29] and Edward *et al.* [30] have recently reported that α-Si_3N_4 prepared by a CVD method and the reaction bonded α-Si_3N_4 had the oxygen contents of 0.300 and 0.26 to 0.53 wt %, respectively. It appears that our experimental evidence supports the results of Priest *et al.* [29].

Airey *et al.* [10] reported that the colour of deposits varied from white to black according to T_{dep} in the $SiH_4 + NH_3/N_2$ (or H_2) and $SiCl_4 + NH_3/N_2$ (or Ar) systems. Galasso *et al.* [17] also reported that the surface varied from white to black and the black surface was obtained when high NH_3/SiF_4 gas ratios were used.

Table I indicates that the variation in colour of the deposits may be attributed to the oxygen content, and both depend on T_{dep} and P_{tot}.

5. Conclusions

(1) Massive amorphous and crystalline Py–Si_3N_4 were successfully prepared. The maximum thickness was 4.2 mm for amorphous deposits and 4.6 mm for crystalline deposits. The structure depended strongly on T_{dep} and P_{tot}. Amorphous deposits were obtained at relatively low T_{dep} of 1100 and 1200° C. At 1300° C, the amorphous deposits were formed at P_{tot} = 10 to 40 and 80 to 300 Torr; the crystalline deposits were obtained at P_{tot} = 40 to 70 Torr. The X-ray diffraction results indicated that crystalline deposits are α-Si_3N_4.

(2) For amorphous deposits, three types of cone structures were observed; i.e. (a) primary pebble-like cones at low T_{dep} and P_{tot}, (b) large primary cones composed of secondary cones at high T_{dep} and high P_{tot}, (c) large primary cones composed of secondary pebble-like cones at the A–C boundary.

(3) The surface of crystalline deposits was composed of oriented small crystals and was markedly affected by P_{tot}.

(4) Thin amorphous deposits were translucent, while thick ones were white. On the other hand, thin crystalline deposits were also translucent, but thick ones varied in colour from black to white depending on oxygen content.

(5) The oxygen content increased with decreasing T_{dep} and P_{tot}. Amorphous deposits contained 1.6 to 2.2 wt % oxygen.

(6) The silicon content was close to a theoretical composition for both deposits.

(7) No segregation of silicon and nitrogen at cone boundaries was detected.

(8) At low T_{dep} and low P_{tot}, amorphous deposits seem to be formed from the liquid state.

Acknowledgements

The authors would like to express their appreciation to Mr Tasaku Sato of Tohoku University for carrying out the electron probe microanalysis, and to Mr Yujiro Miyagawa of Japan Electro Components, Ltd for performing the scanning electron microscope observations.

References

1. K. S. MAZDIYASNI and C. M. COOKE, *J. Amer. Ceram. Soc.* **56** (1973) 628.
2. M. J. GRIECO, F. L. WORTHING and B. SCHWARTZ, *J. Electrochem. Soc.* **115** (1968) 525.
3. T. L. CHU, C. H. LEE and G. A. GRUBER, *ibid* **114** (1967) 717.
4. S. YOSHIKA and S. TAKAYANAGI, *ibid* **114** (1967) 962.
5. S. M. HU, *ibid* **113** (1966) 693.
6. J. V. DALTAN and J. DROBEK, *ibid* **115** (1968) 865.
7. D. N. BROWN, P. V. GRAY, F. K. HEUMANN, H. R. PHILIPP and E. A. TAFT, *ibid* **115** (1968) 311.
8. P. S. SCHAFFER and B. SWAROOP, *Ceram. Bull.* **49** (1970) 536.
9. C. R. BARNES and C. R. GEESNER, *J. Electrochem. Soc.* **107** (1960) 98.
10. A. C. AIREY, S. CLARKE and P. POPPER, *Proc. Brit. Ceram. Soc.* **22** (1973) 305.
11. J. A. ABOAF, *J. Electrochem. Soc.* **116** (1969) 1736.
12. K. E. BEAN, P. S. GLEIN, R. L. YEAKLEY and W. R. RUNYAN, *ibid* **114** (1967) 733.
13. V. Y. DOO, D. R. KERR and D. R. NICHOLS, *ibid* **115** (1968) 61.
14. B. E. DEAL, E. L. MACKENNA and P. L. CASTRO, *ibid* **116** (1969) 997.
15. W. A. KOHLER, *Met. Trans.* **1** (1970) 735.
16. R. C. G. SWANN, R. R. MEHTA and T. P. CAUGE, *J. Electrochem. Soc.* **114** (1967) 713.
17. F. GALASSO, U. KUNTZ and W. J. CROFT, *J. Amer. Ceram. Soc.* **55** (1972) 431.
18. S. M. HU and L. V. GREGOR, *J. Electrochem. Soc.* **114** (1967) 826.
19. M. G. COLLET, *ibid* **116** (1969) 110.
20. H. F. STERLING and R. C. G. SWANN, *Solid State Electronics* **8** (1965) 653.
21. I. KOHATSU and J. E. MCCAULEY, *Mat. Res. Bull.* **9** (1974) 917.
22. R. MARCHAND, Y. LAURENT and J. LANG, *Acta Cryst.* **B25** (1969) 2157.
23. H. SCHAFFER and J. NICKL, *Z. Anorg. Allgem. Chem.* **274** (1953) 250.
24. S. YAJIMA and T. HIRAI, *J. Mater. Sci.* **4** (1969) 416.
25. S. N. RUDDLESDEN, "Special Ceramics 4", edited by P. Popper (British Ceramic Research Association, Stoke-on-Trent, 1968) p.153.
26. S. WILD, P. GRIEVESON and K. H. JACK, "Special Ceramics 5", edited by P. Popper (British Ceramic Research Association, Stoke-on-Trent, 1972) p.385.
27. I. COLQUHOUN, S. WILD, P. GRIEVESON and K. H. JACK, *Proc. Brit. Ceram. Soc.* **22** (1973) 207.
28. H. FELD, P. ETTMAYER and L. PETZENHAUSER, *Ber. Dt. Keram. Ges.* **51** (1974) 127.
29. H. F. PRIEST, F. C. BURNS, G. L. PRIEST and E. C. SKAAR, *J. Amer. Ceram. Soc.* **56** (1973) 395.
30. A. J. EDWARD, D. P. ELIAS, M. W. LINDLEY, A. ATKINSON and A. J. MOULSON, *J. Mater. Sci.* **9** (1974) 516.

Received 3 September and accepted 9 September 1975.